Applied Thermal Engineering 212 (2022) 118514

Contents lists available at ScienceDirect

Applied Thermal Engineering

journal homepage: www.elsevier.com/locate/apthermeng

Research Paper

Novel geometric design of thermoelectric leg based on 3D printing for radioisotope thermoelectric generator

Mingxin Bian [a], Zhiheng Xu [a,b,*], Caifeng Meng [a], Huanyu Zhao [a], Xiaobin Tang [a,b]

[a] Department of Nuclear Science and Technology, Nanjing University of Aeronautics and Astronautics, Nanjing 211106, China
[b] Key Laboratory of Nuclear Technology Application and Radiation Protection in Astronautics, Ministry of Industry and Information Technology, Nanjing 211106, China

ARTICLE INFO

Keywords:
Geometric design
Side area
Heat dissipation
3D printing
Output performance

ABSTRACT

To meet the power supply development needs of electronic devices in spacecraft, the optimized design and fabrication of geometric configuration of thermoelectric (TE) legs to increase the power output of radioisotope thermoelectric generators are proposed. The principle of performance enhancement is the increase of heat dissipation on the increased side area, which is analyzed according to Fourier's law. Helix-shaped and spoke-shaped TE legs with special geometrical shapes are proposed and fabricated by 3D printing technology. The geometric design makes the TE legs produce a larger temperature difference and inevitably brings about an increase in resistance. Variation of TE legs' output performance with the geometrical parameters is analyzed based on the finite element method. Results show that the helix-shaped TE legs with the appropriate geometrical parameters can produce maximum output power of 2.78 mW, which are 2.55 times of the traditional cylinder-shaped TE legs with the same mass. And the spoke-shaped TE legs can produce maximum output power of 2.28 mW, which are 2.09 times of the traditional cylinder-shaped TE legs. Nine TE legs with special shapes and sixteen with traditional shapes are integrated into the same space (16.5 mm × 16.5 mm). The results show that the combination of TE legs with special shapes produce a higher power density, more than 66%–98% compared with traditional shapes due to lighter mass. TE modules with different shapes are fabricated by direct-writing 3D printing technology, and their output performances are tested. TE modules with special shapes exhibit greater open-circuit voltage and output power than the traditional shapes, which are consistent with the simulation results. The simulation and experimental results indicate that the geometric design of TE legs with larger side areas can improve the output performance of TE devices. This design concept of optimizing the geometry to increase the temperature difference can be applied to thermoelectric generators under the condition of natural heat dissipation to improve power output and heat dissipation, and reduce weight.

1. Introduction

With the increase of multifunctional electronic devices with small size, high integration and high energy consumption are equipped in spacecraft [1–3], and more researchers are turning their exploration to deep space [4,5]. However, solar cells cannot satisfy the power consumption of the space spacecraft due to the increasing distance between the spacecraft and the sun [6], and chemical battery with stable output cannot provide long-term power for spacecraft [7,8]. Radioisotope thermoelectric generators (RTGs) are seen as promising power supply devices in deep space exploration due to their long life [9], high stability [10], and compact structure [11,12]. RTGs convert the decay heat of the radioisotope into electricity directly based on the Seebeck effect. However, relatively low conversion efficiency limits their wider application [13,14]. Conversion efficiency can be expressed by $\eta = \frac{T_h - T_c}{T_h} * \frac{\sqrt{1+Z\overline{T}}-1}{\sqrt{1+Z\overline{T}}+T_c/T_h}$, where T_c and T_h represent the temperature of the cold side and hot side of the thermoelectric (TE) legs, respectively, and $\overline{T}$ is the average temperature of the TE legs.ZT is the dimensionless figure of merit that evaluates the TE properties of materials in TE legs; $ZT = \alpha^2\sigma/\kappa$, where Î ± is the Seebeck coefficient, σ is the electrical conductivity, κ is the thermal conductivity, and T is the absolute temperature [15,16]. Thus, to obtain a high conversion efficiency, not only does the ZT value of the materials need to be improved but also the temperature difference (ΔT) between two sides of the TE legs should be increased [17–19]. In the process of heat flowing from the hot side to the cold side in the TE legs, it will dissipate to the surroundings on the side of the TE

* Corresponding author at: Department of Nuclear Science and Technology, Nanjing University of Aeronautics and Astronautics, Nanjing 211106, China.
E-mail address: xuzhiheng@nuaa.edu.cn (Z. Xu).

https://doi.org/10.1016/j.applthermaleng.2022.118514
Received 26 October 2021; Received in revised form 23 March 2022; Accepted 8 April 2022
Available online 18 April 2022

Nomenclature

Sets

RTG	Radioisotope thermoelectric generator
TE	Thermoelectric
FEM	Finite element method
I–V	Current-Voltage
PVP	Polyvinylpyrrolidone
DMF	Dimethyl formamide
1D	One-dimensional
3D	Three-dimensional
Bi_2Te_3	Bismuth telluride

Parameters

η	Conversion efficiency (%)
T_c	Temperature of cold side of TE leg (K)
T_h	Temperature of hot side of TE leg (K)
$\overline{T}$	Average temperature of TE leg (K)
ZT	Figure of merit (a. u.)
α	Seebeck coefficient (μV/K)
σ	Electrical conductivity (S/m)
κ	Thermal conductivity (W/(m·K))
T	Absolute temperature (K)
ΔT	Temperature difference (K)
μ	Shape parameter of TE leg (a. u.)
t	Temperature of differential element of TE leg (K)
t_∞	Temperature of surroundings (K)
x	Distance that heat flows in TE leg (mm)
Φ	Heat generated in differential element of TE leg (W)
λ	Heat transfer coefficient of materials (W/(m·K))
dV	Volume of the differential element of TE leg (mm^3)
Φ_s	Heat dissipation on side of the differential element of TE leg (W)
h	Convective heat transfer coefficient ($W/(m^2 \cdot K)$)
ds	Side area of differential element (mm^2)
dx	Height of differential element (mm)
t_0	Surface temperature of heat source (K)
H	Height of TE leg (mm)
a	Length of rectangle-shaped TE leg (mm)
b	Width of rectangle-shaped TE leg (mm)
R	Radius of the cross section of helix-shaped and cylinder-shaped TE leg (mm)
r	Radius of the helix of helix-shaped TE leg (mm)
n	Number of the helix turns of helix-shaped TE leg (a. u.)
φ	Angle between the orientation of helix-shaped TE leg and direction of heat flow (°)
m	Number of the spokes of spoke-shaped TE leg (a. u.)
θ	Angle of the spokes of spoke-shaped TE leg (°)
r_1	Inner radius of the spoke-shaped TE leg (mm)
r_2	Outer radius of the spoke-shaped TE leg (mm)
V	Voltage (mV)
P	Power (mW)
R_{in}	Resistance of TE leg (mΩ)
R_L	Resistance of load (mΩ)
ρ	Resistivity of materials (m/S)
A	Cross-sectional area of TE leg (mm^2)
V_{oc}	Open-circuit voltage (mV)
P_{max}	Maximum output power (mW)

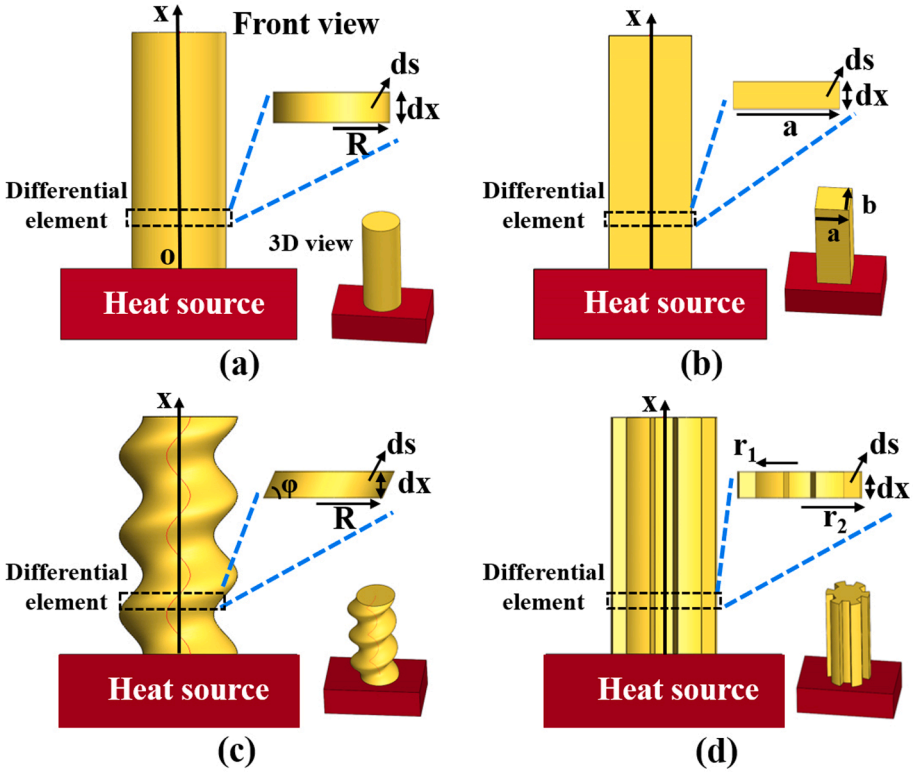

Fig. 1. Schematic view of heat transfer and differential element of TE legs with geometrical shapes of (a) cylinder, (b) rectangle, (c) helix, and (d) spoke.

legs in forms of convective heat transfer and radiative heat transfer. And the amount of heat dissipated into the surroundings by means of convective heat transfer and radiative heat transfer is proportional to the side area of the TE legs. For this reason, TE legs with larger side area due to special geometrical shapes may produce larger ΔT between the hot and cold sides and better conversion efficiency.

Sahin et al. demonstrated that the shape parameter (μ) of TE legs has a substantial influence on conversion efficiency and power generated by the devices [20]. Thimont et al. analyzed the output performance of TE legs with three newly proposed shapes of prismatic, hollow and layer, and the results showed that the TE legs with hollow and layer produce higher voltage than the traditional cylinder [21]. Zebin et al. proposed the variable-angle annular thermoelectric generator, and found that it shows an improvement in output performance under different boundary conditions, compared with conventional constant-angle annular thermoelectric generator [22]. Jhonathan et al. proposed the stretchable helical architecture thermoelectric generator to maintain a greater temperature difference between the hot and cold sides and obtain a greater output power [23]. Khalil et al. studied the TE conversion performance of TE legs with different geometrical shapes of the same volume using the finite element method (FEM) and found that the Y-leg produces a greater conversion efficiency under the same hot junction of the cross-sectional area [24]. In the research on the geometric configuration of TE legs, the TE legs with high output performance have larger side area due to special geometrical shapes for heat dissipation to a certain extent.

Traditional preparation methods, including hot pressing and spark plasma sintering, can only fabricate TE legs with regular shapes, such as cylinder and cuboid [25–28]. These shapes have definite side areas, and their contributions to the ΔT between the two sides of TE legs are limited. With the application of 3D printing technology to TE materials in recent years, it has become a simple, low-cost preparation method for TE legs with complex shapes [29,30]. Su et al. prepared in-plane and annular TE devices with excellent TE properties and good output performance using direct-writing 3D printing technology [31]. Abu et al. fabricated trapezoidal-shaped and rectangular-shaped TE legs with dispenser printing technology, and the trapezoidal-shaped TE prototype generates better electrical output than the rectangular-shaped prototype [32]. Improvement of the performance of TE legs derived from the optimal design of geometry provides new inspirations for the development of RTGs.

In this work, two design methods of the TE legs' geometric configuration were proposed, based on the increment of side area to enhance heat dissipation under the condition of natural heat dissipation. Compared with the previous research works on the geometry of the TE legs, TE legs with special geometrical shapes proposed in this work have larger side areas for heat dissipation, and the enhancement in output performance is also more obvious. The principle of performance enhancement was analyzed according to Fourier Law. The enhancement effect of geometrical parameters on the output performance of the TE legs was studied using the FEM. Comparison of output performance of the combination of TE legs with different geometrical shapes and numbers was carried using FEM. TE legs with traditional and newly proposed geometrical shapes were fabricated by 3D printing technology and connected to TE modules, and their output performance was tested. The consistency of simulation and experimental results prove that TE legs with special geometrical shapes can produce greater output performance by increasing the side area.

2. Design method and experiment

2.1. Heat conduction analysis of TE legs

Fig. 1 shows that during the conversion from heat into electricity, heat flows along the axial direction of the TE legs, which can be analyzed by the one-dimensional (1D) Fourier law of heat conduction as follows [33]:

$$\frac{d^2t}{dx^2}+\frac{\Phi}{\lambda}= \tag{1}$$

where t is the temperature of differential element; x is the distance that heat flows; Φ is the heat generated in the differential element, which is negative because only heat dissipation exists in TE legs; and λ is the heat transfer coefficient of the TE materials in TE legs.

For TE legs, the heat generated in the differential element can be expressed as follows:

$$\Phi = -\frac{\Phi_s}{dV} \tag{2}$$

where dV is the volume of the differential element, and Φ_s is the heat dissipation on the side of the differential element, which can be expressed as follows:

$$\Phi_s = h\hat{A}\cdot(t-t_\infty)ds \tag{3}$$

where h is the convective heat transfer coefficient, ds is the side area of the differential element, and t and t_∞ represent the temperature of the differential element and the surroundings, respectively. To simplify the mathematical model, the λ and h of the TE materials in the TE legs are assumed to be constants, and the temperature effect of λ and h are neglected. The temperature distribution in the differential elements is uniform. What's more, the amount of heat dissipated into the surroundings by means of radiative heat transfer is much less than that of convective heat transfer. Therefore, the radiative heat transfer that occurs on the side of the TE legs is included in the convective heat transfer by setting h to a slightly larger value [34,35].

The cold and hot sides of the TE legs can be defined by boundary conditions. For the hot side,

$$t = t_0|_{x=0} \tag{4}$$

where t_0 is the surface temperature of the heat source. The temperature of the hot side is the same as the surface temperature of the heat source. For the cold side,

$$-\lambda(\frac{dt}{dx})|_{x=H} = h(t-t_\infty) \tag{5}$$

where H is the height of the TE leg. The top surface of the TE legs dissipates heat to the surroundings by means of convective heat transfer. And the temperature of the cold side can be obtained by solving the heat conduction equation with boundary conditions [36].

TE legs with different geometrical shapes exhibit diverse heat transfer effects due to the difference in the side area of the differential elements, as shown in Fig. 1. For TE legs with traditional shapes of cylinder and rectangle, as shown in Fig. 1(a) and 1(b), respectively, the heat dissipation on their differential elements can be expressed as follows:

$$\Phi_{cylinder} = -\frac{2h(t-t_\infty)}{R} \tag{5}$$

$$\Phi_{rectangle} = -\frac{2(a+b)h(t-t_\infty)}{ab} \tag{6}$$

TE legs with helix-shaped and spoke-shaped specific geometric configuration were proposed, as shown in Fig. 1(c) and 1(d), respectively, and the heat dissipation on their differential elements can be simplified as follows:

$$\Phi_{helix} = -\frac{2h(t-t_\infty)}{R}\hat{A}\cdot\frac{2}{\pi cos\varphi} \tag{7}$$

$$\Phi_{spoke} = -2h(t-t_\infty)[\frac{m\theta r_2+(360-m\theta)r_1}{m\theta r_2^2+(360-m\theta)r_1^2}+\frac{360m(r_2-r_1)}{\pi[m\theta r_2^2+(360-m\theta)r_1^2]}] \tag{8}$$

where R is the radius of the cross section of the helix-shaped and

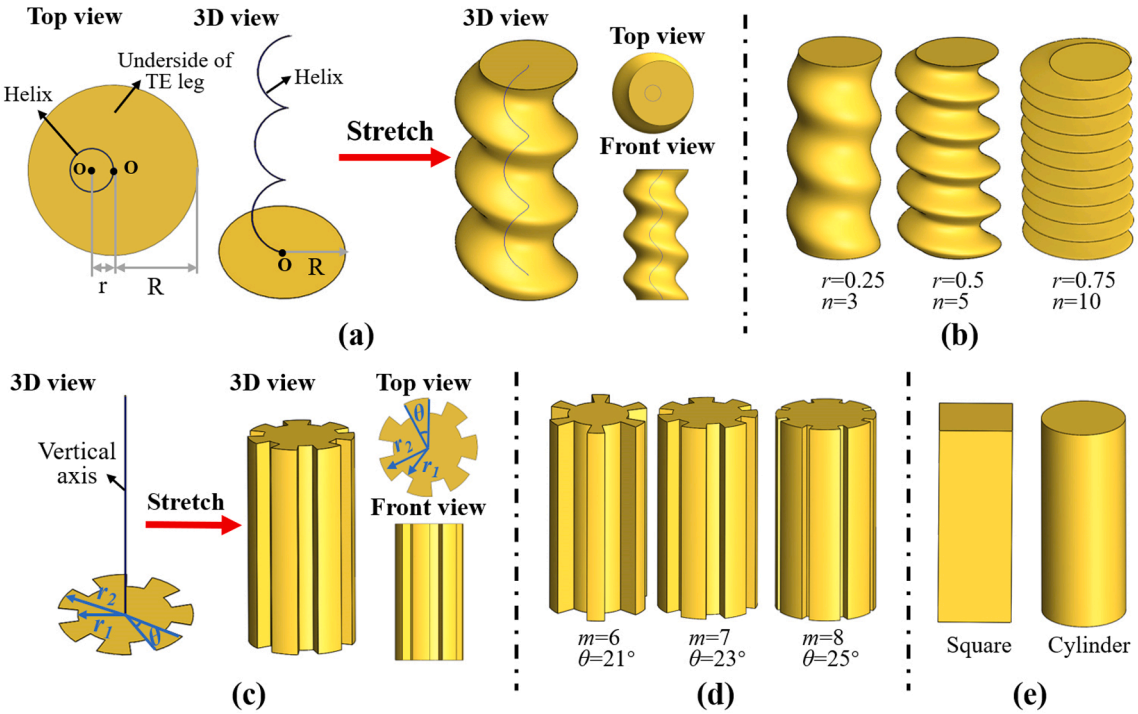

Fig. 2. Schematic diagram of TE legs with different geometrical shapes. (a) Design method of helix-shaped TE legs; (b) Helix-shaped TE legs with different r, n; (c) Design method of spoke-shaped TE legs; (d) Spoke-shaped TE legs with different r_1, m and θ; (e) Traditional square-shaped (left) and cylinder-shaped (right) TE legs.

cylinder-shaped TE legs; a and b are the length and width of the rectangle-shaped TE legs, respectively; φ is the angle between the orientation of the helix-shaped TE legs and the direction of heat flow; m and θ are the number and angle of the spokes of the spoke-shaped TE legs, respectively; and r_1 and r_2 are the inner radius and outer radius of the spoke-shaped TE legs, respectively. As shown in Equations (7) and (8), the differential elements of the helix-shaped and spoke-shaped TE legs can dissipate more heat to the surroundings on the increased side areas, compared with traditional cylinder-shaped and rectangle-shaped TE legs.

The generated voltage (V) of the TE legs can be calculated as follows:

$$V = \alpha \hat{A} \cdot \Delta T \tag{9}$$

and the power (P) of the TE legs can be calculated according to Ohm's law:

$$P = \left(\frac{V}{R_{in} + R_L}\right)^2 R_L \tag{10}$$

where α is the Seebeck coefficient of the materials in TE legs; ΔT is the temperature difference between the hot and cold sides of the TE legs; R_{in} and R_{L} are the resistance of TE legs and load, respectively, and the output power can reach the maximum when $R_{\text{in}} = R_{\text{L}}$.

Power is determined by voltage and resistance together. However, the resistance of TE legs with special shapes is affected by its geometrical parameters. The resistance of cylinder-shaped, spoke-shaped, and rectangle-shaped TE legs can be expressed as [37]:

$$R_{in} = \rho \frac{H}{A} \tag{11}$$

Where ρ is the resistivity of the materials in TE legs; H and A are the height and cross-sectional area of TE legs, respectively. TE legs with three geometrical shapes have the same formula for R_{in} because the movement direction of the carriers inside them is the same as the heat flow. For the helix-shaped TE leg, it can modify to [33]:

$$R_{in} = \rho \frac{H}{A cos\varphi} \tag{12}$$

The helix-shaped and spoke-shaped TE legs proposed in the current work have larger side areas based on two methods: 1) producing an angle between the orientation of TE legs and the direction of heat flow, 2) increasing the perimeter of the cross profile of TE legs. The heat dissipation that occurs on the side of the TE legs is enhanced due to the increased side area, and the ΔT between the hot and cold sides also increases. Compared with traditional cylinder and rectangle, the helix-shaped and spoke-shaped TE legs with optimized geometrical parameters can considerably increase output performance.

2.2. Design method

Fig. 2(a) shows the design of the helix-shaped TE legs that is formed by the underside in the horizontal plane stretched along a helix. Notably, the underside stretches vertically along the helix, and the underside is always parallel to the horizontal plane but not perpendicular to the helix. And the radius of the cross section of the helix-shaped TE legs and the radius of the helix are set to R and r, respectively. Therefore, this geometric structure has the same volume and mass as a cylinder with the same bottom area and height, that is, the r and the number (n) of the helix turns do not affect the volume and mass of the TE legs if the bottom area and height are fixed. Moreover, the helix-shaped TE legs with different n and r are shown in Fig. 2(b). The contributions of the r and n to the output performance of the TE legs were studied.

The spoke-shaped TE legs are formed by a pattern in the horizontal plane stretched vertically along an axis, and the axis is perpendicular to the pattern, as shown in Fig. 2(c). The side area of the spoke-shaped TE legs is increased by increasing the perimeter of the pattern in the horizontal plane, and the perimeter is determined by the inner (r_1) and outer (r_2) radius, and the number (m) and angle (θ) of the spokes. Fig. 2(d) shows spoke-shaped TE legs with different r_1, m and θ. The contribution of various geometrical parameters to the enhancement of output performance of the TE legs was further analyzed.

Table 1
Geometrical parameters of various TE legs.

Geometrical parameters	Helix-shaped	Spoke-shaped	Square-shaped	Cylinder-shaped
Geometrical variables	n = 1–15 r = 0.25–1.5 mm	m = 5–9 θ = 21°–25°	–	–
Constant	H = 10 mm R = 2 mm	H = 10 mm r_2 = 2.25 mm	H = 10 mm a = 3.544 mm	H = 10 mm R = 2 mm

Note: r_1 changes with the m and θ of the spokes in the spoke-shaped TE legs.

To study the improvement of the output performance caused by the special geometry, the cylinder-shaped and square-shaped (for rectangle-shaped TE legs, when $a = b$) TE legs with the same bottom area and height (with the same mass and volume) were selected as the control group. For all TE legs, the height (H) was set to 10 mm. The bottom of the cylinder-shaped and helix-shaped TE legs was a circle with a radius of 2 mm. The side length of the square-shaped TE legs was set to 3.544 mm. For the spoke-shaped TE legs, r_2 was set to 2.25 mm, and r_1 varied with m and θ to have the same bottom area (12.56 mm^2) as the other TE legs. The contribution of different geometrical parameters to the enhancement of output performance was studied in detail, and the geometrical parameters are shown in Table 1.

COMSOL Multiphysics software based on the FEM was used to simulate the conversion of heat into electricity. Fig. S1 in Supplementary Material shows TE legs with different geometrical shapes established in COMSOL. A cuboid with a surface temperature is kept constant of 400 K was used as a heat source. In the simulation, the TE legs and heat source were opened to the surroundings with a temperature of 293.15 K, and the TE legs dissipate heat into the surroundings by means of natural convection heat dissipation. The TE properties of Bismuth Telluride (Bi_2Te_3) based TE material used in COMSOL are shown in Fig. S2 and Table S1.

2.3. Experimental preparations and testing

Preparation and molding of TE slurry: Direct-writing 3D printing technology was used to manufacture TE legs with specific geometrical shapes. Polyvinylpyrrolidone (PVP) and dimethyl formamide (DMF) were used as organic binder and volatile solvent, respectively, due to their excellent viscosity and non-toxicity. P-type $Bi_{0.5}Sb_{1.5}Te_3$ and N-type $Bi_2Se_{0.3}Te_{2.7}$ powders (Chengdu Alfa Metal Material Co., Ltd, China) with particle sizes of less than 10 μm were used as TE fillers. PVP was dissolved in DMF to form a uniform colloid solution by mechanical stirring, and then TE powders were added to the above solution in batches. Stirring continued until most of the DMF was evaporated and TE powder was evenly dispersed in the solution to form a stable TE slurry. The above preparation method was inspired by Su et al.'s work [31]. After many attempts, the mass ratio of DMF, PVP, and TE powders was determined to be 2:1:25. This TE slurry have a suitable viscosity and modulus to print objects with special shapes. Fig. 3(a) depicts the preparation of TE slurry. The TE slurry was molded into different shapes by Adventure 3D-LB-Printer (Shenzhen Adventuretech Co., Ltd., China). The slurry was loaded into a syringe, where the diameter of the needle was 260 μm. The other side of the syringe was connected to an air compressor, and the flow rate of the slurry was controlled by air pressure. The moving path, speed of the needle and the extrusion of slurry were controlled by the computer control system in a layer-by-layer deposition fashion. The TE slurry was printed on a glass substrate. The as-3D-printed TE legs were dried at 120 °C in a drying oven for 24 h, and then annealed at 450 °C for 6 h in a tube furnace flowing a mixture of gas of 15% H_2 and 85% Ar. The reducing atmosphere can remove the oxide layer on the surface of TE legs and increase conductivity. The 3D printing process is shown in Fig. 3(b).

Combination and performance testing of TE legs: The sintered TE legs were combined into a single TE module consisting of N-type and P-type TE legs to test the output performance. The TE legs were assembled on a glass substrate with a thickness of 1 mm using conductive silver glue.

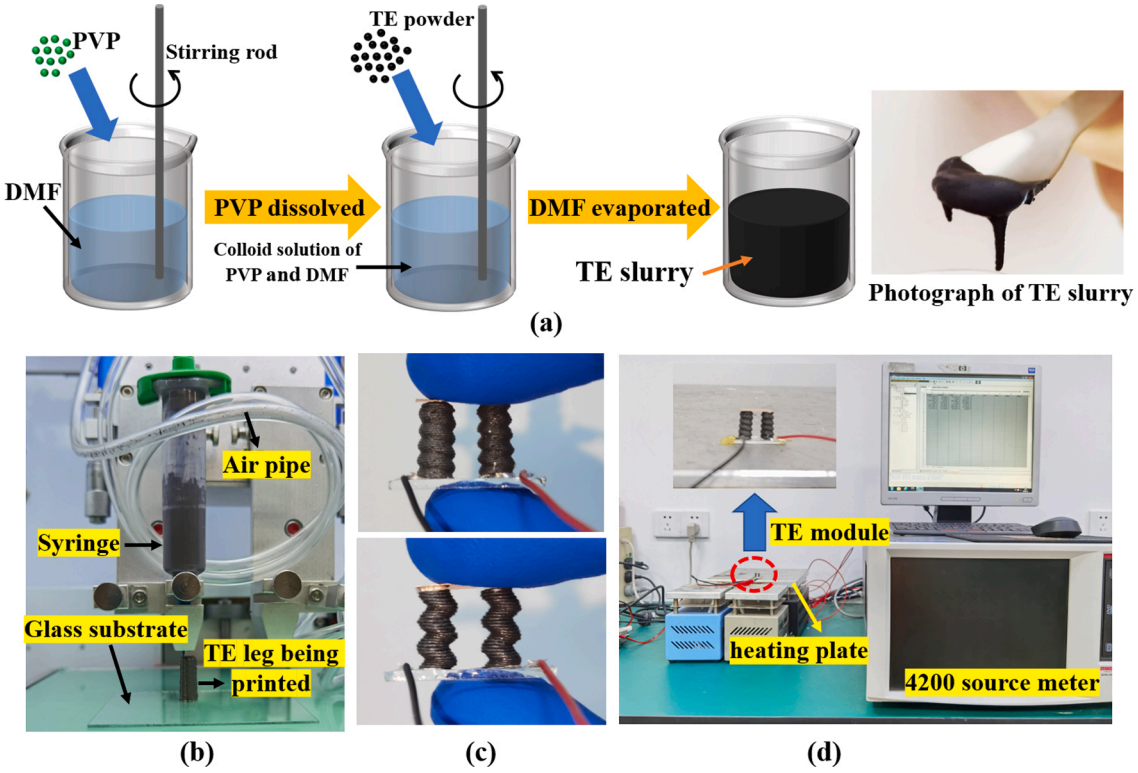

Fig. 3. (a) Schematic diagram of preparation of TE slurry; (b) Photograph of 3D printing process; (c) Photograph of manufactured TE modules with shape of helix of "r = 0.25, n = 5" (top), and "r = 0.5, n = 3" (bottom); (d) Electrical output performance measurement system.

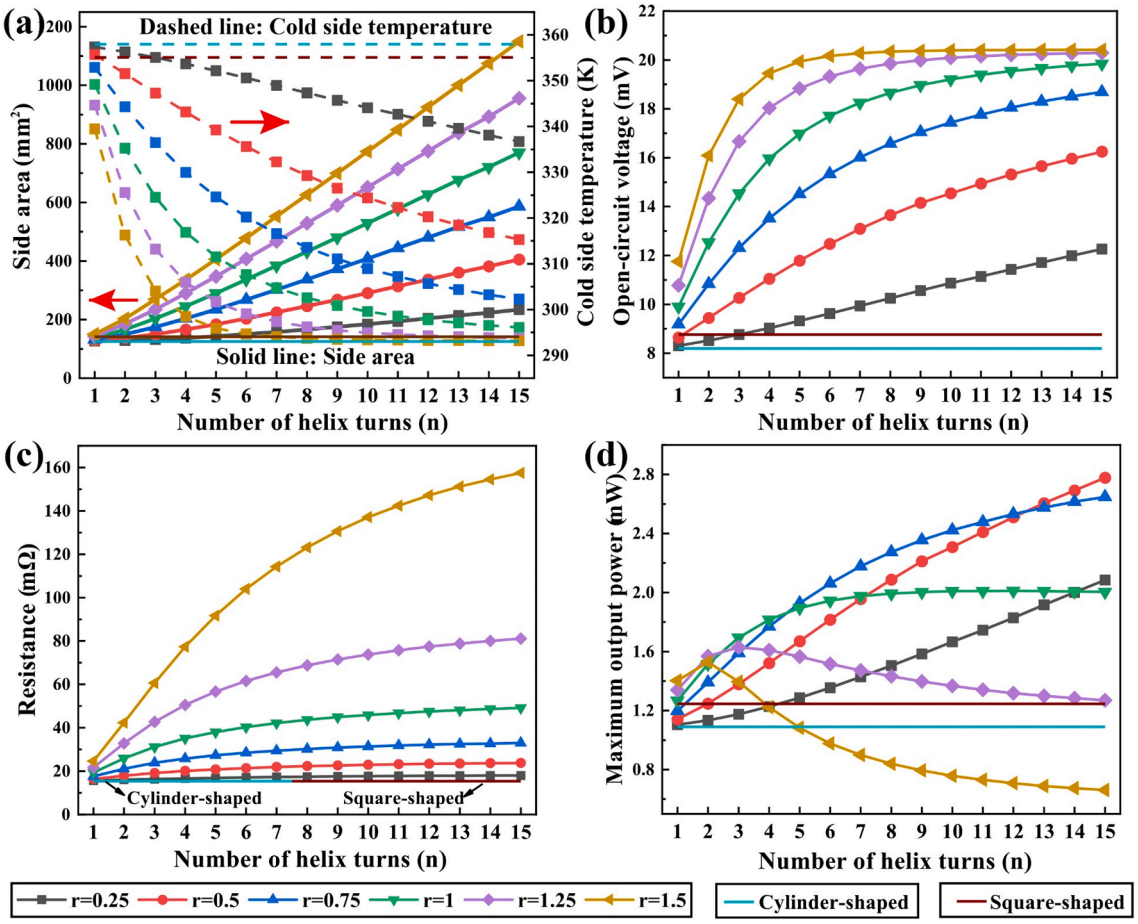

Fig. 4. Variation of output performance of helix-shaped TE legs with the helix radius (r) and number (n) of helix turns. (a) Side area and cold side temperature, (b) Open-circuit voltage, (c) Resistance, and (d) Maximum output power.

Copper sheets were used as an electrode to connect the P-type and N-type TE legs. An electric heating plate was used as the heat source, and the surface temperature can be set artificially. Keithley 4200 source meter was used to test the Current-Voltage (I–V) characteristic curves of the TE modules.

3. Result and discussion

In the simulation, the variation trend of output performance of the helix-shaped and spoke-shaped TE legs with the geometrical parameters was studied, and the output performance comparison of the TE legs with different geometrical shapes integrated in the same volume was carried out. In the confirmatory experiment, TE legs with different geometrical shapes were fabricated by direct-writing 3D printing technology and connected into a π-shaped module, and the I–V characteristic curves under heat source with different temperatures were tested to verify the correctness of the simulation works.

3.1. Helix-shaped TE legs

The temperature and voltage diagram of the helix-shaped TE legs with different geometrical parameters are shown in Figs. S3 and S4, and the variation of output performance with geometrical parameters is shown in Fig. 4.

Fig. 4(a) shows that the side area of the helix-shaped TE legs increases linearly with the number (n) of helix turns, and the rate of increase rises with helix radius (r), which is determined by its geometrical properties. The temperature of the cold side decreases as n increases, and the rate of decrease increases with r, which is due to the increments of radiant and convective heat dissipation that occur on the increased side area. For different r, a corresponding n can reduce the temperature of the cold side to the surroundings temperature of 293.15 K. Traditional cylinder-shaped and square-shaped TE legs have small side areas for heat dissipation; thus, the cold side temperature is higher than the helix-shaped TE legs with all geometrical parameters. The ΔT between the hot and cold sides is converted into voltage based on the Seebeck effect, and the changing trend of open-circuit voltage (V_{oc}) with n is opposite to that of the cold side temperature, as shown in Fig. 4(b). The cylinder-shaped and square-shaped TE legs produce the lowest V_{oc}. In general, the helix-shaped TE legs have larger side areas for heat dissipation, so they can generate larger ΔT and V_{oc} under the condition of natural heat dissipation. And the traditional cylinder-shaped and square-shaped TE legs generate the lowest ΔT and V_{oc} due to the smaller heat dissipation occurred on the smaller side areas.

However, the change of geometry prolongs the path of carriers, which lead to an increase in resistance as shown in Fig. 4(c). Similarly, resistance increases as n increases, and the rate of increase is proportional to r that can be explained by Equation (12). The output power of TE leg is determined by voltage and resistance together, and the trend of change is shown in Fig. 4(d). Output power has a tendency of increasing first and then decreasing as n increases, that is, a peak is observed here. At the same time, the n at the peak value appears decreases as r increases. For example, the peak values appear at $n = 7$, 3, 2, when $r = 1$, 1.25, 1.5 mm, respectively. The n that the peak values appear may exceed 15 when r is less than 1 mm because the inclination (φ) between the orientation of TE leg and the direction of heat flow increases as n increases, and the side area and resistance increase accordingly. The enhancement effect of voltage on output power exceed the reduction

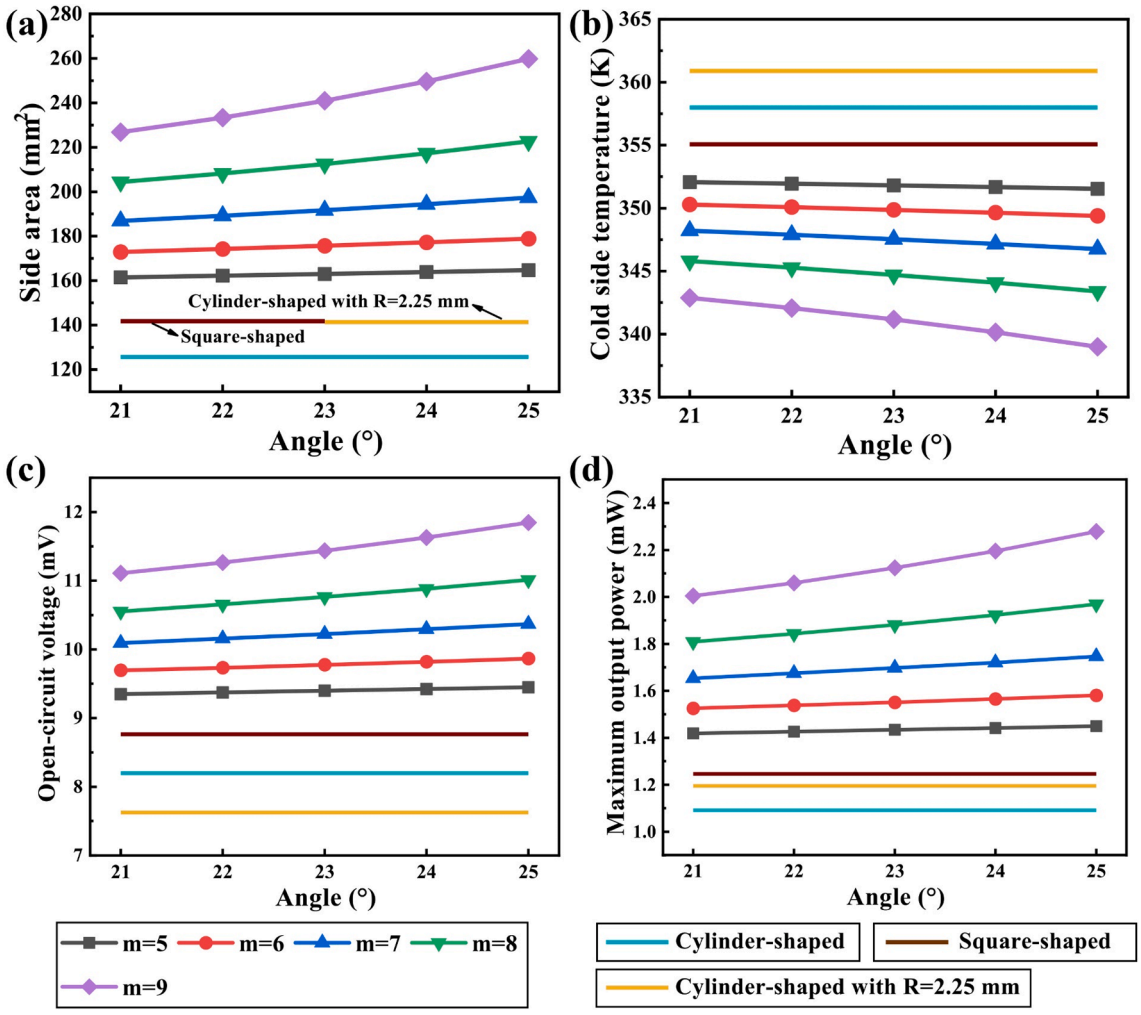

Fig. 5. Variation of output performance of spoke-shaped TE legs with angle (θ) and number (m) of spokes. (a) Side area; (b) Cold side temperature; (c) Open-circuit voltage; and (d) Maximum output power.

effect of resistance; hence, output power shows a trend of increasing with the increase of n (before the peak value appear). However, as n continues to increase, the reduction effect of resistance on output power exceed voltage, resulting in a decrease in output power. Moreover, φ increases as r increases; thus, the n at which the enhancement effect of voltage is equal to the reduction effect of resistance would decrease as r increases, that is, the n at which the peak of output power appear decreases as r increases. Therefore, the output power of the helix-shaped TE legs has a maximum value for different r, which exceed that of the traditional cylinder-shaped and square-shaped TE legs. In the current simulation work, the helix-shaped TE legs can produce the maximum output power of 2.78 mW when the geometrical parameters are "$r = 0.5$, $n = 15$", which exceed 155% of the cylinder-shaped TE legs (1.09 mW) and 124% of the square-shaped TE legs (1.24 mW).

3.2. Spoke-shaped TE legs

The temperature and voltage diagram of the spoke-shaped TE legs with different geometrical parameters are shown in Figs. S5 and S6, and the variation of output performance with geometrical parameters is shown in Fig. 5.

Fig. 5 shows the variation trend of the output performance of spoke-shaped TE legs with angle (θ) and number (m) of spokes, and cylinder-shaped and square-shaped TE legs with the same bottom area, as well as the cylinder-shaped TE legs with a radius of $R = 2.25$ mm (the same as the outer radius r_2) as the control group. Fig. 5(a) shows that the side areas of the spoke-shaped TE legs are higher than that of the TE legs in the control group due to the contribution of the spoke. Side area increases as θ, and the rate of increase rises with the number (m) of spokes. The increase in side area leads to a decrease in the temperature of the cold side, which is attributed to the increased heat dissipation on the side area. The cold side temperature of all spoke-shaped TE legs are lower than that of the three traditional shapes, as shown in Fig. 5(b). However, the contribution of the spoke to the increase of side area and the decrease in temperature of the cold side is limited, and the cold side temperatures of all spoke-shaped TE legs are higher than the surroundings temperature.

Notably, spoke-shaped TE legs have the same resistance ($R_{in} = 115$ mΩ) as cylinder-shaped and square-shaped ones due to the same bottom area and moving path of carriers. The cylinder-shaped TE legs with a radius of $R = 2.25$ mm has a smaller resistance (108 mΩ) due to the larger bottom area. Ultimately, maximum output power (P_{max}) shows a trend similar to that of V_{oc} as shown in Fig. 5(d). The output performance of spoke-shaped TE legs exceed that of traditional shapes, even the cylinder-shaped ones with larger mass. Unlike helix-shaped ones, the output performance of spoke-shaped TE legs increases as m and θ increase, and no peak value is observed, that is, m and θ of the spokes should be as large as possible for greater power output. In current simulation work, the spoke-shaped TE legs with the best parameters of "$m = 9$, $\theta = 25°$" can produce the power of 2.28 mW, which exceed 109% of the cylinder-shaped TE legs (1.09 mW) and 84% of the square-shaped TE legs (1.24 mW).

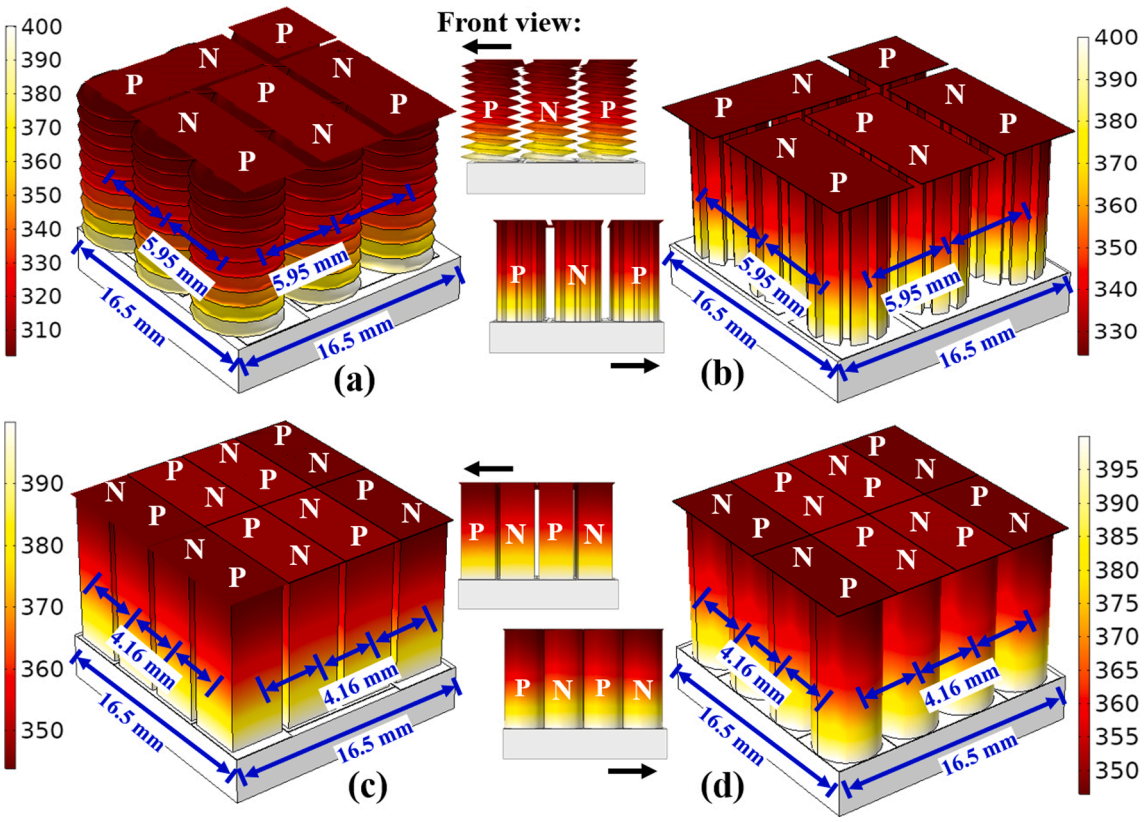

Fig. 6. Temperature diagram of integrated TE legs in COMSOL. (a) Helix-shaped; (b) Spoke-shaped; (c) Square-shaped; and (d) Cylinder-shaped.

Table 2
Output performance of integrated TE legs.

Output parameters	Helix-shaped	Spoke-shaped	Cylinder-shaped	Square-shaped
V_{oc}/mV	146.79	115.00	142.31	148.86
R_{in}/mΩ	212.06	109.31	186.74	186.69
P_{max}/mW	24.92	30.49	28.24	31.10
Power density/ mW/g	3.15	3.75	1.89	2.07

3.3. Integrated output performances

The arrangement of TE legs with different geometrical shapes and numbers will affect the output performance of TE devices in the same volume. FEM was used for further analysis. The helix-shaped TE legs with "$r = 0.75$, $n = 10$" and the spoke-shaped with "$m = 9$, $\theta = 25°$" were selected as the research objects. The traditional cylinder-shaped and square-shaped TE legs with the same bottom area were used as control. These TE legs were integrated in a space of 16.5 mm × 16.5 mm with a manner of series, as shown in Fig. 6.

For the helix-shaped and spoke-shaped TE legs, nine TE legs are connected in series with a center distance of 5.95 mm, and five P-type and four N-type are shown in Fig. 6(a) and 6(b). As for the traditional square-shaped and cylinder-shaped TE legs, sixteen TE legs are connected with a center distance of 4.16 mm, and the number of P-type and N-type is 8 shown, as in Fig. 6(c) and 6(d). The output performance of integrated TE legs with different shapes is summarized in Table 2, and the corresponding voltage diagrams are shown in Figs. S7.

The voltage generated by the helix-shaped TE legs is comparable with that of the traditional shaped ones due to the increased heat dissipation on the increased side area, although the number is only 9. The spoke-shaped TE legs generate lower voltage due to the limitation of number and side area. The extension of the carrier path leads to a substantial increase in resistance of the helix-shaped TE legs, and the spoke-shaped TE legs have the lowest internal resistance due to the number of TE legs and unchanged carrier path. In general, spoke-shaped TE legs produce a power output equivalent to that of the traditional shapes, but helix-shaped ones produce slightly less power output. Notably, the power density of TE legs with special geometrical shapes far exceed that of traditional shapes, and even increased by 66% and 98% when the helix-shaped and spoke-shaped TE legs are compared with cylinder-shaped ones. Traditional cylinder-shaped and square-shaped TE legs have the same internal resistance, and the square-shaped ones generate a slightly higher voltage due to the larger side area. Therefore, the output power and power density of the square-shaped TE legs are slightly higher than that of the cylinder-shaped TE legs.

3.4. Output performance test of TE module

Five TE modules with geometrical parameters in the above simulation work were tested, including two helix-shaped with parameters of "$r = 0.25$, $n = 5$" and "$r = 0.5$, $n = 3$", one spoke-shaped with the parameter of "$m = 6$, $\theta = 25°$" and the cylinder-shaped and square-shaped. Fig. 7(a) shows the TE modules with different geometrical shapes fabricated by 3D printing technology, and the corresponding TE modules constructed in COMSOL are shown in Fig. 7(b). The height of the TE modules in the experiment and simulation is 10 mm. A heating plate was used as the heat source in the test system. The surface temperature changed from 353.15 K to 393.15 K, which was used to study the output characteristics of the TE modules. The TE modules were placed on the heating plate, and the cold side was in surroundings of 300.5 K for natural heat dissipation, as shown in Fig. 3(d).

Fig. 8 describes the variation of the maximum output power (P_{max}) generated by the TE modules with different geometrical shapes under different heat source temperatures in the experimental and simulation results, and the *I-V* characteristic curves of the TE modules under the

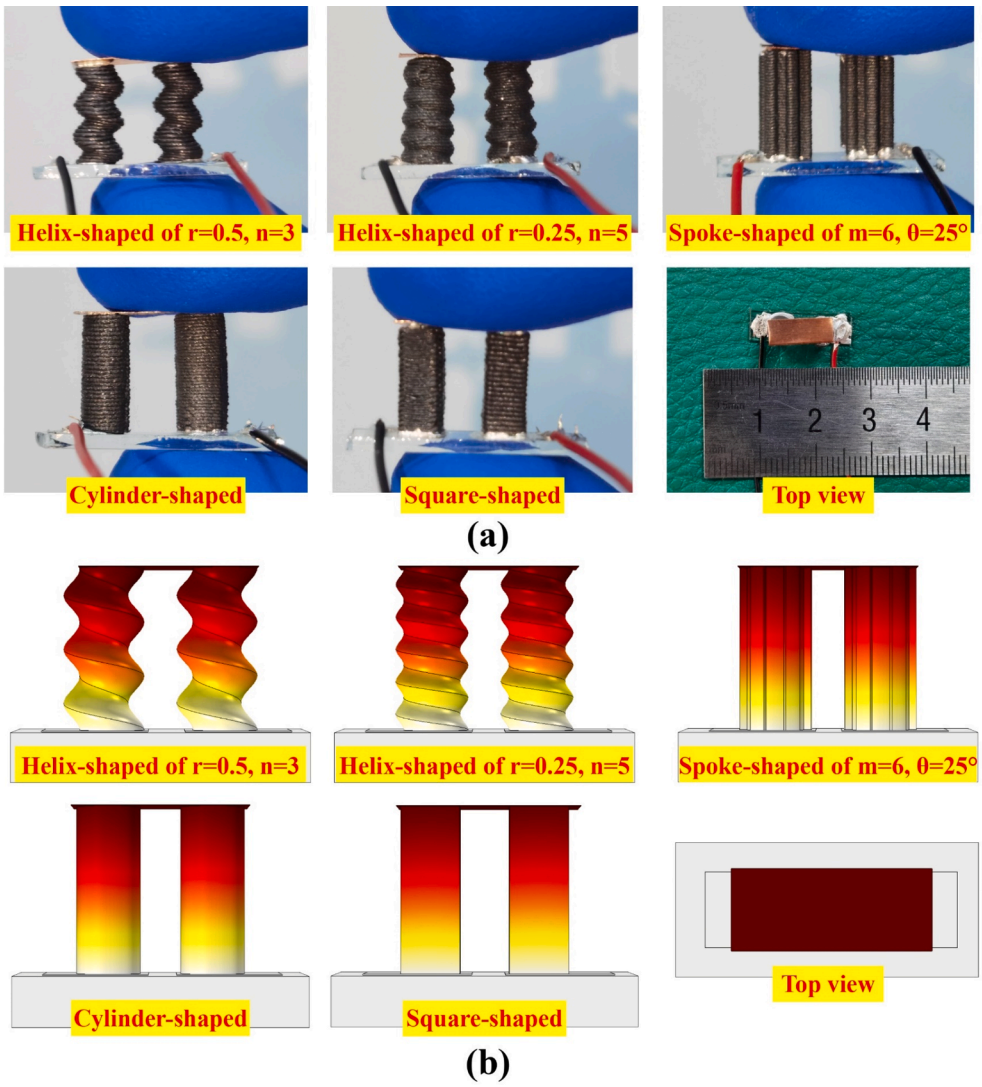

Fig. 7. (a) Photograph of TE modules with different geometrical shapes fabricated by 3D printing technology, (b) the corresponding TE modules constructed in COMSOL.

heat source temperature of 393.15 K. The variation of the open-circuit voltage (V_{oc}) of the TE modules under different heat source temperatures in the experimental and simulation results are shown in Fig. S8, and the *I-V* characteristic curves of the TE modules under the heat source temperatures of 353.15 K, 363.15 K, 373.15 K and 383.15 K are shown in Fig.S9. In the experimental and simulation results, the P_{max} and V_{oc} of the TE modules with all geometrical shapes increase with the temperature of the heat source increases. The increase of the V_{oc} is because the temperature difference (ΔT) between the hot and cold sides increases with the temperature of heat source increases, and the P_{max} also increases as the heat source temperature increases due to the V_{oc}. The variation of the output performance of the TE modules with all geometrical shapes as the heat source temperature shows the same trend in the experimental and simulation results. And the P_{max} of TE modules with different geometrical shapes in the experimental and simulation results are summarized in Table 3 when the temperatures of the heat source are 353.15 K and 393.15 K.

The TE modules with geometrical shapes of helix and spoke exhibit greater output performance in the experimental results compared with the traditional cylinder-shaped and square-shaped TE modules, which is consistent with the simulation results. For example, when the temperature of heat source is 393.15 K, the experimental results show that the spoke-shaped TE module with "$m = 6$, $\theta = 25°$" and the helix-shaped TE module with "$r = 0.5$, $n = 3$" generate the P_{max} of 2.73 and 2.55 μW respectively, which exceed the traditional cylinder-shaped TE module of 2.05 μW by 33.2% and 24.4%. The simulation results show that spoke-shaped TE module with "$m = 6$, $\theta = 25°$" and the helix-shaped TE module with "$r = 0.5$, $n = 3$" generate the P_{max} of 3.44 and 3.05 mW respectively, which exceed the cylinder-shaped TE module of 2.61 mW by 31.8% and 16.9%. The performance improvement between the TE modules with special and traditional geometrical shapes shows the same magnitude in the experimental and simulation results. However, the output performance of the TE modules in the experimental results are lower than the simulation results, and the square-shaped TE module shows a greater output performance than the cylinder-shaped ones, which is somewhat different from the experimental results. This is because the properties of the TE materials, the geometrical structure of TE legs, and the heat dissipation process occurred on the side of TE leg were idealized in the simulation. And the environment where the TE modules located is not as stable as in the simulation. What's worse, the conductive silver glue has a significant impact on the output performance of the TE modules, and the electrical contact resistance and thermal contact resistance are not considered in the simulation work. And the P_{max} of TE modules with different geometrical shapes in the experimental and simulation results are summarized in Table S3 when the temperatures of the heat source are 363.15 K, 373.15 K and 383.15

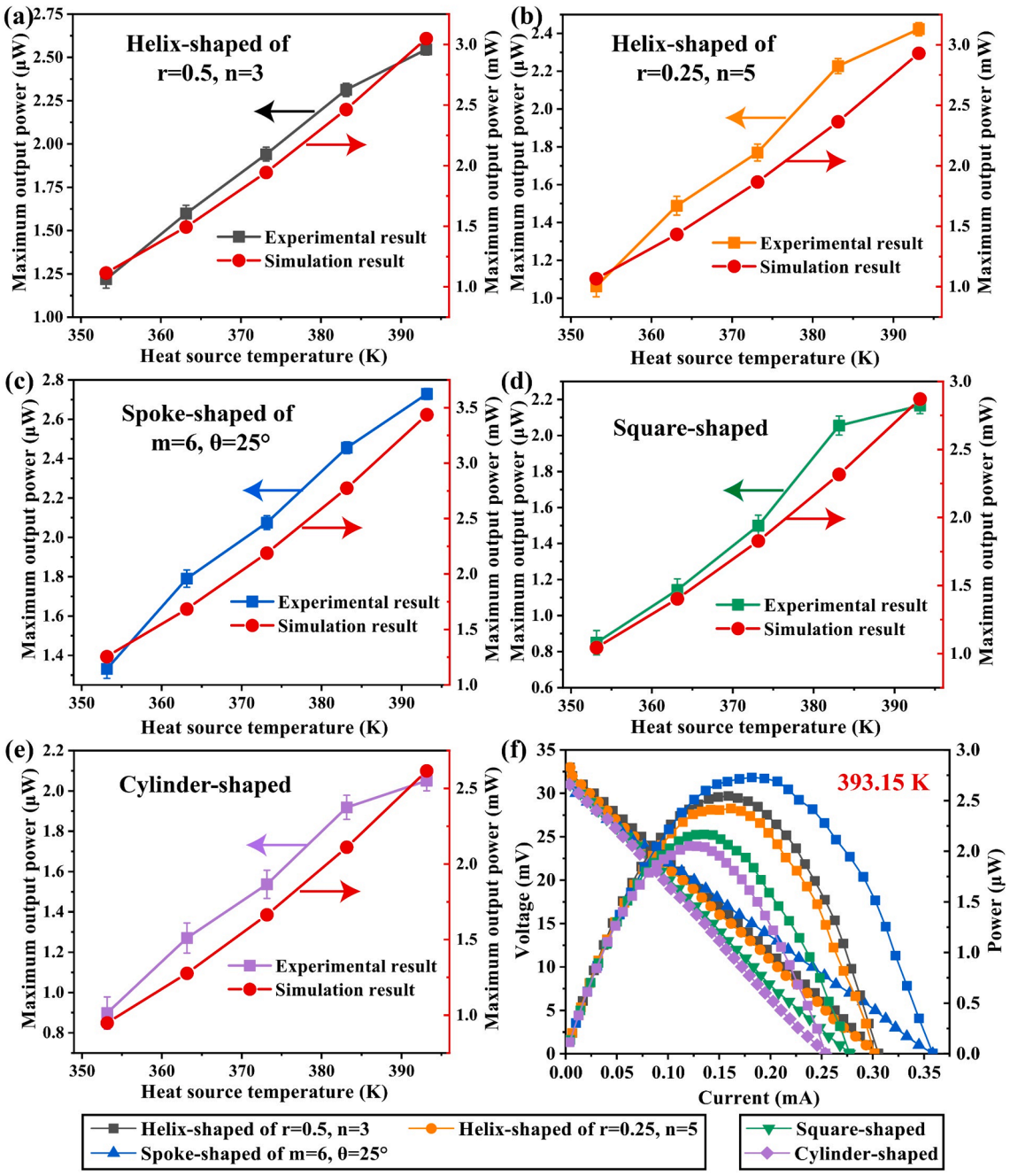

Fig. 8. Maximum output power of TE modules with different geometrical shapes in the simulation and experimental results under different heat source temperatures, (a) Helix-shaped of $r = 0.5$, $n = 3$, (b) Helix-shaped of $r = 0.25$, $n = 5$, (c) Spoke-shaped of $m = 6$, $\theta = 25°$, (d) Square-shaped, (e) Cylinder-shaped; (f) *I–V* characteristic curves of TE modules under the heat source temperature of 393.15 K.

K.

The improvement of output performance between TE modules with special and traditional shapes in the experimental results is consistent with the simulation results, and output performance increases as the side area. This result also verifies that by increasing the side area of the TE legs, the heat dissipation effect under natural heat dissipation conditions is improved, thereby enhancing the output performance of the TE legs.

4. Conclusions

This work proposes a new geometric design concept to improve the output voltage and power of the TE legs in RTGs based on increasing side area to enhance heat dissipation caused by convective heat transfer and radiative heat transfer. Helix-shaped and spoke-shaped TE legs with different geometrical shapes are designed, where the helix-shaped TE legs are based on producing an angle between the direction of heat flow and the orientation of TE leg, and the spoke-shaped TE legs are based on increasing the perimeter of cross profile. The helix-shaped TE legs have a larger side area and can generate a larger temperature difference and voltage than the traditional cylinder-shaped and square-shaped TE legs, but the extension of the carrier path leads to an increase in resistance due to geometrical properties. Optimal geometrical parameters are needed for the helix-shaped TE legs to produce the best output power. For the spoke-shaped TE leg, the resistance does not change with geometrical parameters, and the number and angle of the spokes should be as much as possible to obtain the optimal power output. In the

Table 3
Maximum power of TE modules.

Temperature	P_{max}	Helix-shaped of r = 0.5, n = 3	Helix-shaped of r = 0.25, n = 5	Spoke-shaped of m = 6, θ = 25°	Cylinder-shaped	Square-shaped
353.15 K	Exp/μW	1.22	1.06	1.33	0.90	0.85
	Sim/mW	1.11	1.07	1.25	0.95	1.04
393.15 K	Exp/μW	2.55	2.42	2.73	2.05	2.17
	Sim/mW	3.05	2.93	3.44	2.61	2.87

COMSOL simulation, the helix-shaped and spoke-shaped TE legs with best geometrical parameters can generate the maximum output power of 2.78 and 2.28 mW, respectively, which exceed the cylinder-shaped with same mass by 155% and 109%, respectively.

Sixteen TE legs with traditional shapes and nine with special shapes are integrated into the same volume. The combination of the TE legs with special shapes produces the voltage and resistance slightly lower than the traditional shapes due to the limitation of quantity, but the output power is similar to the traditional shapes due to the increase in voltage of each TE leg. Finally, the power densities of the helix-shaped and spoke-shaped TE legs exceed that of the cylinder-shaped TE legs by 66% and 98%, respectively, due to less quantity and mass. Therefore, the combination of TE legs with special shapes can produce sufficient output performance with lighter mass, which can be applied in scenarios where the weight of power supply is limited.

TE modules with special geometrical shapes show greater output performance under different heat source temperatures than traditional shapes. The consistency of the experimental and simulation results shows that optimizing the geometry of TE leg to increase the side area, thereby enhancing heat dissipation on the side area, can improve performance output. Moreover, TE legs with more complex geometrical shapes still bring a little difficulty to the fabrication, although the helix-shaped and spoke-shaped TE legs have been fabricated by 3D printing technology. At the same time, considering the temperature of the heat source and the power requirements of the electronic equipment, there are more geometrical parameters, such as the helix radius (r), the number (n) of helix turns, and the number (m) and angle (θ) of the spokes of the TE legs need to be optimized to achieve good heat dissipation effects and output performance. This design concept of optimizing the geometry of TE leg can be applied to improve power output, conversion efficiency, heat dissipation and reduce weight, especially for the radioisotope thermoelectric generators and other TE generators under the condition of natural heat dissipation.

CRediT authorship contribution statement

Mingxin Bian: Conceptualization, Writing – review & editing, Software. **Zhiheng Xu:** Validation. **Caifeng Meng:** Data curation, Methodology. **Huanyu Zhao:** Software, Investigation. **Xiaobin Tang:** Validation.

Declaration of Competing Interest

The authors declare that they have no known competing financial interests or personal relationships that could have appeared to influence the work reported in this paper.

Acknowledgements

This work was supported by the National Natural Science Foundation of China (Grant No. 12005101), the Shanghai Aerospace Science and Technology Innovation Project (Grant Nos. SAST2019-112 and SAST2020-097).

Appendix A. Supplementary data

Supplementary data to this article can be found online at https://doi.org/10.1016/j.applthermaleng.2022.118514.

References

[1] N. Meyer, Laptops in space: a sparing analysis case study for personal computers used in deep space exploration, 2019 Annu. Reliab. Maintainab. Symp., IEEE (2019) pp. 1–6.
[2] Massaro Tieze, L.C. Liddell, Santa Maria, S. Bhattacharya, BioSentinel: a biological CubeSat for deep space exploration, Astrobiology (2020).
[3] I. Levchenko, K. Bazaka, T. Belmonte, M. Keidar, S. Xu, Advanced materials for next-generation spacecraft, Adv. Mater. 30 (2018) 1802201.
[4] W. Wu, W. Liu, D. Qiao, D. Jie, Investigation on the development of deep space exploration, Sci. China Technol. Sci. 55 (4) (2012) 1086–1091.
[5] B.E. Crucian, A. Choukèr, R.J. Simpson, S. Mehta, G. Marshall, S.M. Smith, S. R. Zwart, M. Heer, S. Ponomarev, A. Whitmire, Immune system dysregulation during spaceflight: potential countermeasures for deep space exploration missions, Front. Immunol. 9 (2018) 1437.
[6] G.L. Matloff, Deep space probes: To the outer solar system and beyond, Springer Science & Business Media, 2006.
[7] P. Nie, S.W. Zhang, A. Ran, C. Yang, S. Chen, Z. Li, X. Zhang, W. Deng, T. Liu, F. Kang, Full-cycle electrochemical-thermal coupling analysis for commercial lithium-ion batteries, Appl. Therm. Eng. 184 (2021), 116258.
[8] M. Carbone, A. Sajadi, K. Loparo, Bifurcation analysis of dc electric power systems for deep space exploration spacecraft, 2019 IEEE Power Energy Conf. Illinois, IEEE (2019) pp. 1–7.
[9] M. Prelas, M. Boraas, F.D.L.T. Aguilar, J.D. Seelig, M.T. Tchouaso, D. Wisniewski, Nuclear batteries and radioisotopes, Springer, 2016.
[10] V.V. Gusev, A.A. Pustovalov, N.N. Rybkin, L.I. Anatychuk, B.N. Demchuk, I. Y. Ludchak, Milliwatt-power radioisotope thermoelectric generator (RTG) based on plutonium-238, J. Electron. Mater. 40 (5) (2011) 807–811.
[11] Z. Yuan, X. Tang, Z. Xu, J. Li, W. Chen, K. Liu, Y. Liu, Z. Zhang, Screen-printed radial structure micro radioisotope thermoelectric generator, Appl. Energy. 225 (2018) 746–754.
[12] K. Liu, Y. Liu, Z. Xu, Z. Zhang, Z. Yuan, X. Guo, Z. Jin, X. Tang, Experimental prototype and simulation optimization of micro-radial milliwatt-power radioisotope thermoelectric generator, Appl. Therm. Eng. 125 (2017) 425–431.
[13] C.S.R. Matthes, D.F. Woerner, T.J. Hendricks, J.P. Fleurial, K.I. Oxnevad, C.D. Barklay, J.F. Zakrajsek, Next-generation radioisotope thermoelectric generator study, 2018 IEEE Aerosp. Conf., IEEE (2018) pp. 1–9.
[14] K. Liu, X. Tang, Y. Liu, Z. Xu, Z. Yuan, D. Ji, S. Ramakrishna, Experimental optimization of small–scale structure–adjustable radioisotope thermoelectric generators, Appl. Energy. 280 (2020), 115907.
[15] Q. Ma, H. Fang, M. Zhang, Theoretical analysis and design optimization of thermoelectric generator, Appl. Therm. Eng. 127 (2017) 758–764.
[16] C.N. Kim, Development of a numerical method for the performance analysis of thermoelectric generators with thermal and electric contact resistance, Appl. Therm. Eng. 130 (2018) 408–417.
[17] M.A. Zoui, S. Bentouba, J.G. Stocholm, M. Bourouis, A review on thermoelectric generators: progress and applications, Energies. 13 (2020) 3606.
[18] Z. Soleimani, S. Zoras, B. Ceranic, S. Shahzad, Y. Cui, A review on recent developments of thermoelectric materials for room-temperature applications, Sustain. Energy Technol. Assessments. 37 (2020), 100604.
[19] Fitriani, R. Ovik, B.D. Long, M.C. Barma, M. Riaz, M.F.M. Sabri, S.M. Said, R. Saidur, A review on nanostructures of high-temperature thermoelectric materials for waste heat recovery, Renew. Sustain. Energy Rev. 64 (2016) 635–659.
[20] A.Z. Sahin, B.S. Yilbas, The thermoelement as thermoelectric power generator: Effect of leg geometry on the efficiency and power generation, Energy Convers. Manag. 65 (2013) 26–32.
[21] Y. Thimont, S. LeBlanc, The impact of thermoelectric leg geometries on thermal resistance and power output, J. Appl. Phys. 126 (2019) 95101.
[22] Z. Weng, F. Liu, W. Zhu, Y. Li, C. Xie, J. Deng, L. Huang, Performance improvement of variable-angle annular thermoelectric generators considering different boundary conditions, Appl. Energy. 306 (2022), 118005.
[23] J.P. Rojas, D. Singh, D. Conchouso, A. Arevalo, I.G. Foulds, M.M. Hussain, Stretchable helical architecture inorganic-organic hetero thermoelectric generator, Nano Energy. 30 (2016) 691–699.
[24] Al. Khalil, A. Elhassnaoui, S. Yadir, O. Abdellatif, Y. Errami, S. Sahnoun, Performance comparison of TEGs for diverse variable leg geometry with the same leg volume, Energy 224 (2021).
[25] G.-E. Lee, I.-H. Kim, Y.S. Lim, W.-S. Seo, B.-J. Choi, C.-W. Hwang, Preparation and thermoelectric properties of Bi_2Te_3-Bi_2Se_3 solid solutions, J. Korean Phys. Soc. 64 (10) (2014) 1416–1420.
[26] N. Bolghanabadi, S.A. Sajjadi, A. Babakhani, Y. Saberi, Effects of synthesis parameters and thickness on thermoelectric properties of Bi_2Te_3 fabricated using mechanical alloying and spark plasma sintering, J. Electron. Mater. 50 (3) (2021) 1331–1339.

[27] R. Cao, Z. Zhu, X.J. Li, X. Hu, H. Song, Enhanced thermoelectric properties of the Lu-doped and CNT-dispersed Bi_2Te_3 alloy, Appl. Phys. A. 125 (2019) 126.
[28] H. You, Z. Li, Y. Shao, X. Yuan, W. Liu, H. Tang, Q. Zhang, Y. Yan, X. Tang, Flexible Bi_2Te_3-based thermoelectric generator with an ultra-high power density, Appl. Therm. Eng. 202 (2022) 117818, https://doi.org/10.1016/j.applthermaleng.2021.117818.
[29] M. Orrill, S. LeBlanc, Printed thermoelectric materials and devices: Fabrication techniques, advantages, and challenges, J. Appl. Polym. Sci. 134 (2017).
[30] M.S. Hossain, T. Li, Y. Yu, J. Yong, J.H. Bahk, E. Skafidas, Recent advances in printable thermoelectric devices: materials, printing techniques, and applications, RSC Adv. 10 (2020) 8421–8434.
[31] N. Su, P. Zhu, Y. Pan, F. Li, B. Li, 3D-printing of shape-controllable thermoelectric devices with enhanced output performance, Energy. 195 (2020), 116892.
[32] A.R.M. Siddique, S. Mahmud, Van Heyst, Performance comparison between rectangular and trapezoidal-shaped thermoelectric legs manufactured by a dispenser printing technique, Energy. 196 (2020), 117089.
[33] M. Kaviany, Heat transfer physics, Cambridge University Press, 2014.
[34] K. Qiu, A.C.S. Hayden, Development of a thermoelectric self-powered residential heating system, J. Power Sources. 180 (2) (2008) 884–889.
[35] S. Shittu, G. Li, Q. Xuan, X. Xiao, X. Zhao, X. Ma, Y.G. Akhlaghi, Transient and non-uniform heat flux effect on solar thermoelectric generator with phase change material, Appl. Therm. Eng. 173 (2020), 115206.
[36] F. Kreith, R.M. Manglik, Principles of heat transfer, Cengage learning (2016).
[37] W.M. Rohsenow, J.P. Hartnett, Y.I. Cho, Handbook of heat transfer, McGraw-Hill New York, 1998.